Eleventh International Conference on CFD in the Minerals and Process Industries
CSIRO, Melbourne, Australia
7-9 December 2015

EXPERIMENTAL AND NUMERICAL INVESTIGATION OF A MICRO-STRUCTURED BUBBLE COLUMN WITH CHEMISORPTION

Krushnathej THIRUVALLUVAN SUJATHA[1*], **Deepak JAIN**[1†], **Satish KAMATH**[1‡], **J. A. M. KUIPERS**[1§], **Niels G. DEEN**[1¶]

[1]Department of Chemical Engineering and Chemistry, Eindhoven University of Technology, P.O. Box 513, 5600MB Eindhoven, The Netherlands

[*] E-mail: k.thiruvalluv.sujatha@tue.nl
[†] E-mail: djiitdjpr@gmail.com
[‡] E-mail: s.kamath@tue.nl
[§] E-mail: j.a.m.kuipers@tue.nl
[¶] E-mail: n.g.deen@tue.nl

ABSTRACT

Bubble columns reactors are often used for gas-liquid contacting processes, for instance in gas-treating processes for H_2S and/or CO_2 removal. The limiting step in the chemisorption process is usually the mass transfer from the gas phase to the liquid phase. The mass transfer rate is a function of the interfacial area, the intrinsic mass transfer coefficient and the driving force. The mass transfer rate can be increased by increasing the interfacial area and/or the interfacial mass transfer coefficient. This can be achieved by means of adding internals such as sieve plates, porous plates, and static mixers (SMV). The addition of internals is also known to reduce the back-mixing in bubble column reactors, which can be advantageous in some situations. In this work, the internals are wire-meshes and serve the purpose of cutting the bubbles. The bubble cutting generates smaller bubbles leading to an increase in gas-liquid interfacial area.

In our previous work, three hydrodynamic regimes were identified for bubbly flow in a micro-structured bubble column (MSBC) with wire mesh (Sujatha *et al.*, 2015). These studies were performed for an air-water system with superficial gas velocities ranging from 5 to 50 mm/s. The effect of the wire mesh layouts on bubble cutting was studied for the case without physical absorption/reaction. The scope of the current research is to extend the work for the case of chemisorption of CO_2 into a $NaOH$ solution, by a combined experimental and simulation approach. Bubble size distribution, pH and holdup data are obtained from chemisorption experiments. These data are compared with simulation results obtained from a detailed VOF-DBM model developed by Jain *et al.* (2014).

Keywords: Micro-Structured Bubble Column, Digital Image Analysis, $CO_2 - NaOH$ system, wire mesh, pH measurement .

NOMENCLATURE

Greek Symbols

ε	Gas holdup, [-].
μ	Dynamic viscosity, [kg/ms].
σ	Surface tension, [-].
ρ	Density, [kg/m^3].

Latin Symbols

d	Diameter, [m].
W	Width, [m].
H	Height, [m].
D	Depth, [m].
A	Area, [m^2].
V	Volume, [m^3].
h	height of liquid-gas dispersion, [m^2].
u	Velocity, [m/s].
Sh	Sherwood number, [-].
Re	Reynolds number, [-].
Sc	Schmidt number, [-].

Sub/superscripts

eq	Equivalent.
b	Bubble.
g	Gas.
l	Liquid.
f	Fluid.
w	Wire.
k	Index k.
H	height expansion.
DIA	Digital Image Analysis.
F	Final.
0	Initial.

INTRODUCTION

Bubble columns are often used for gas-liquid contacting processes, for instance in gas-treating processes for H_2S and/or CO_2 removal. The limiting step in the chemisorption process is usually the mass transfer from the gas phase to the liquid phase. The mass transfer rate is a function of the interfacial area, the intrinsic mass transfer coefficient and the driving force. The mass transfer rate can be increased by increasing the interfacial area and/or the interfacial mass transfer coefficient. This can achieved by means of adding internals such as sieve plates, porous plates, and static mixers (SMV) (Baird, 1992; Deen *et al.*, 2000). The addition of internals is also known to reduce the back-mixing in the bubble column reactor, which can be advantageous in some situations. In our previous work, we have proposed a novel micro-structured bubble column(MSBC) reactor with wire-meshes as internals (Sujatha *et al.*, 2015; Jain *et al.*, 2013, 2014). Jain *et al.* (2013, 2014) have developed a combined VOF-DBM model to simulate and study the effect of wire mesh in the MSBC reactor. Sujatha *et al.* (2015) have done experiments in laboratory scale MSBC

Mesh #	diameter (mm)	opening (mm)	open area (%)
4	0.80	5.5	76
6	0.55	3.6	76
6	0.90	3.3	62
8	0.50	2.7	71
10	0.31	2.2	75
12	0.31	1.8	73
18	0.22	1.1	71

Table 1: Overview of different wire meshes used for experiments

reactor to study the effect of wire mesh configuration and superficial gas velocity. Three hydrodynamic regimes were identified for bubbly flow in a MSBC with wire mesh in an air-water system for superficial gas velocities in the range of 5 to 50 mm/s.

The scope of the current paper is to extend the work for the chemisorption of CO_2 into a $NaOH$ solution, by a combined experimental and simulation approach. Bubble size distribution, pH and holdup data are obtained from chemisorption experiments. These data are compared with simulation results obtained from a detailed VOF-DBM model developed by Jain *et al.* (2014).

This paper is organized as follows. The description of the experimental setup and methods used for obtaining the results (i.e. digital image analysis technique and VOF-DBM method) are discussed elaborately. The results and discussion section consists of visual analysis, experimental results and comparison of experiments with simulation.

MATERIAL AND METHODS

A flat pseudo-2D bubble column reactor of dimensions (width W=0.2 m, depth D=0.03 m, height H=1.3 m) is chosen for experiments. The reactor walls are constructed of transparent glass to enable visual observation by the eye or using a camera. The gas is fed into the column via a group of fifteen gas needles centrally arranged in the distributor plate. The needles have a length (L) = 50 mm, inner diameter (I.D.) = 1 mm and outer diameter (O.D.) = 1.5875 mm. The needles extend 10 mm above the bottom plate and are spaced with a center-to-center distance of 9 mm. An array of five needles is classified as a group, and each group of needles is connected to a mass flow controller. Subsequently, three mass flow controllers are used to control the gas flow rates in the column. Micro-structuring in the reactor is realized by means of thin wires of various dimensions arranged in a mesh structure or by using a Sulzer packing (SMV). The wire mesh or Sulzer packing can be mounted onto the column by using a modular insert, designed for this purpose. The modular insert design allows full flexibility to attach one or more wire meshes at different locations of the insert. The dimensions of the column including the insert are as follows: width=0.14 m, depth=0.03 m, height=1.3 m. The location of the wire mesh was fixed for the experiments at a distance of 0.26 m from the bottom distributor plate and the Sulzer packing is fixed at 0.24 to 0.26 m. An overview of the several mesh configurations can be seen in Table 1.

The experimental procedure followed for the $CO_2 - NaOH$ system is as follows. The column is filled with a well stirred solution of sodium hydroxide prepared with pH = 12.5. Inert gas nitrogen is used to aerate the column before the starting time of the experiment at desired gas flow rate. The camera is focused to a particular section of the column to capture sharp images. The pH meter is immersed in the $NaOH$ solution, at the top of the column to measure and record local pH for the duration of reaction. The flow is switched to CO_2 and the timer is started. Initial liquid height is noted down at time t = 0 and the high-speed recording of images is started. As the reaction proceeds the change in height of gas-liquid dispersion is noted down. Once there is no relevant change in pH with time the CO_2 flow is switched back to nitrogen flow. The change in the gas holdup is observed via the change in height of the gas-liquid dispersion with time.

Digital Image Analysis

The DIA technique (Lau *et al.*, 2013a,b) was developed to determine the mean diameter d_{eq}, bubble size distributions and gas holdup in pseudo-2D bubble column reactor. Sujatha *et al.* (2015) improved the DIA technique to detect very small bubbles. The image analysis algorithm has four main operations: a) Image filtering b) separation of bubbles into solitary and overlapping bubbles c) segmentation of overlapping bubbles using watershedding technique d) combination of solitary and overlapping bubble images. Image filtering involves operations to obtain a desired image involving removal of the inhomogeneous illumination using an Otsu filter (Otsu, 1975). The Otsu filter determines the threshold for separating the bubbles from the background, by thresholding individual blocks of an image. The edges of the bubbles are detected by a Canny edge detection algorithm. The images are separated into solitary bubbles and overlapping bubbles using roundness as a separation criteria. The images with solitary bubbles are segmented by marking the bubbles whereas the overlapping bubbles are segmented using the watershed algorithm proposed by Meyer (1994). An example image after bubble detection is shown in Fig. 1.

A CMOS camera with resolution of 2016 *pixel* $\times$ 2016 *pixel* is used to capture the images of two-phase bubbly flow by using back-lighting to obtain maximum contrast between the bubbles and the background. The MSBC is divided into three different sections for the purpose of imaging and 4000 images are made at 50 Hz for each section . Images from each section have a size of 0.21 m$\times$0.14 m and a small overlap of 0.04 m. The resolution of the image is 0.11 mm/pixel.

The Sauter mean diameter of an image is calculated from the equivalent diameter using the following equation:

$$d_{32} = \frac{\sum_{k=0}^{n} d_{eq,k}^3}{\sum_{k=0}^{n} d_{eq,k}^2} \tag{1}$$

The probability density function (PDF) for a particular bubble diameter class is the ratio of number of bubbles in a particular diameter class(Δd_{eq}) to the sum of number of bubbles in all size classes. Therefore, the PDF of a particular

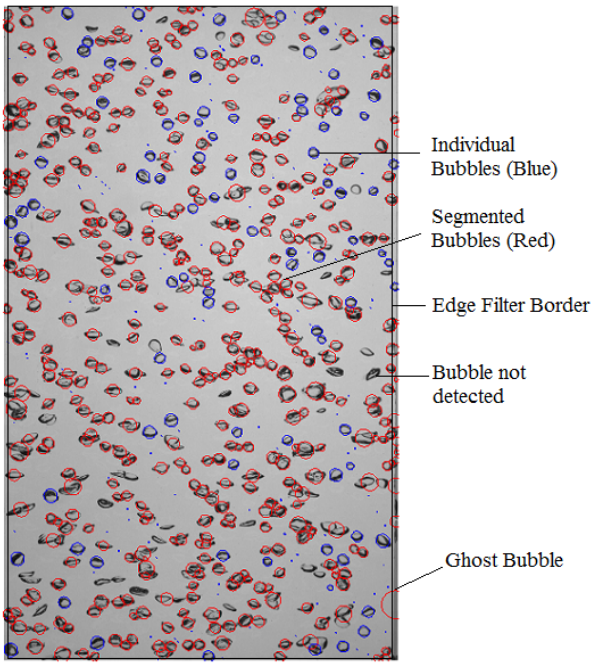

Figure 1: Image after detection. Individual bubbles are indicated by blue circles and segmented bubbles are indicated by red circles.

size class(Δd_{eq}) is calculated from the number of bubbles and average bubble diameter as follows:

$$PDF_{\Delta d_{eq}} = \frac{N_{\Delta d_{eq}}}{\sum_{\Delta d_{eq,min}}^{\Delta d_{eq,max}} N_{\Delta d_{eq,k}}} \tag{2}$$

The gas holdup is determined for the air-water system by liquid expansion measurements. It is calculated by the following formula:

$$\varepsilon_{(g,H)} = \frac{h_f - h_0}{h_f} \tag{3}$$

Where h_f is the height of the gas-liquid dispersion and h_0 is the initial height of the liquid.

VOLUME OF FLUID - DISCRETE BUBBLE MODEL

A Volume of Fluid (VOF) - Discrete Bubble Model (DBM) is used to model the hydrodynamics of the system. This model is an Euler-Lagrangian model. The bubbles are tracked and the liquid phase is treated as a continuum. A force balance is solved for every bubble using Newton's second law of motion. For an incompressible bubble the equations are given by:

$$\rho_b \frac{d(V_b)}{dt} = (\dot{m}_{l\to b} - \dot{m}_{b\to l}) \tag{4}$$

$$\rho_b V_b \frac{d(\mathbf{v})}{dt} = \Sigma\mathbf{F} - (\rho_b \frac{d(V_b)}{dt})\mathbf{v} \tag{5}$$

$$\Sigma\mathbf{F} = \mathbf{F_G} + \mathbf{F_p} + \mathbf{F_D} + \mathbf{F_L} + \mathbf{F_{VM}} + \mathbf{F_W} \tag{6}$$

The forces considered on the bubble are due to gravity ($\mathbf{F_G}$), local pressure gradients ($\mathbf{F_p}$), liquid drag ($\mathbf{F_D}$), lift forces($\mathbf{F_L}$), virtual mass forces($\mathbf{F_{VM}}$) and wall forces ($\mathbf{F_W}$). Closures for these forces are given in the work of Jain *et al.* (2013).

Fluid phase hydrodynamics

The whole system is divided into four phases, each with its own volume fraction (ε): a) liquid (ε_l), b) bubble (ε_b), c) gas (ε_g, continuous layer above the liquid height), and d) wire-mesh (ε_w solid).
Where the sum of all volume fractions equals unity:

$$\varepsilon_l + \varepsilon_g + \varepsilon_b + \varepsilon_w = 1 \tag{7}$$

The liquid phase hydrodynamics is described by the volume averaged Navier-Stokes equations, which consists of continuity and momentum equations:

$$\frac{\partial(\rho_f \varepsilon_f)}{\partial t} + \nabla\cdot(\varepsilon_f \rho_f \mathbf{u}) = (\dot{M}_{b\to l} - \dot{M}_{l\to b}) \tag{8}$$

$$\begin{aligned}\frac{\partial}{\partial t}(\rho_f \varepsilon_f \mathbf{u}) + (\nabla\cdot\varepsilon_f\rho_f\mathbf{uu}) = &-\varepsilon_f\nabla p + \rho_f\varepsilon_f\mathbf{g} \\ &- \mathbf{f}_\sigma - \mathbf{f_{l\to b}} + \mathbf{f_{w\to l}} \\ &+ \{\nabla\cdot\varepsilon_f\mu_{eff}[((\nabla\mathbf{u}) + (\nabla\mathbf{u})^T) \\ &- \frac{2}{3}\mathbf{I}(\nabla\cdot\mathbf{u})]\}\end{aligned} \tag{9}$$

Where

$$\varepsilon_f = \varepsilon_l + \varepsilon_g \tag{10}$$

$$\mu_{eff} = \mu_{L,l} + \mu_{T,l} \tag{11}$$

$\dot{M}$ represents the rate of mass transfer. $\mathbf{f}_\sigma$ represents the local volumetric surface tension force acting on the free surface at the top of the column and $\mathbf{u}$ represents the average fluid velocity. The interface can be seen in Fig. 2.

A Volume of Fluid (VOF) method is used to simulate the free surface and the gas above the liquid level in the column. van Sint Annaland *et al.* (2005) have used this method to successfully show the coalescence of two gas bubbles in a fluid. The grid size used here is larger compared to direct numerical simulations but this is acceptable as the surface only has a small curvature. The local average ρ and μ are calculated using a color function F which is governed by:

$$\frac{DF}{Dt} = \frac{\partial F}{\partial t} + (\mathbf{u}\cdot\nabla F) = 0 \tag{12}$$

$$F = \frac{\varepsilon_l}{\varepsilon_l + \varepsilon_g} = \frac{\varepsilon_l}{\varepsilon_f} \tag{13}$$

It can be easily noted that the grid cells lying completely below the free surface have $\varepsilon_g = 0$ and similarly the grid cells lying completely above the free surface have $\varepsilon_l = 0$. The properties like density and viscosity for the other grid cells that cover the free surface are calculated as follows.

$$\rho_f = F\rho_l + (1-F)\rho_g \tag{14}$$

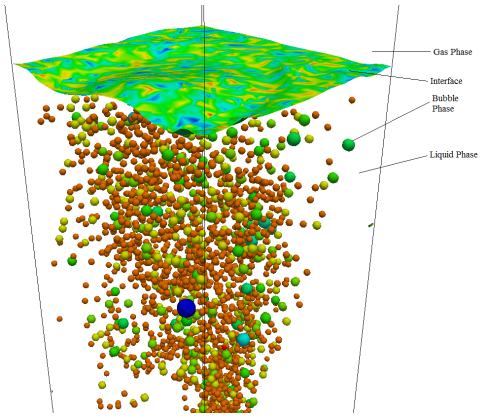

Figure 2: Example snapshot of VOF-DBM simulation showing bubbles and free surface. Note: the geometry differs from the one used in this work.

$$\frac{\rho_f}{\mu_f} = F\frac{\rho_l}{\mu_l} + (1-F)\frac{\rho_g}{\mu_g} \tag{15}$$

The boundary conditions are applied using a flag matrix concept. Fig. 3 shows the different values of the flags of the pseudo 2-D column. The cells are assigned different flag values indicating different types of boundary conditions that are listed in Table 2.

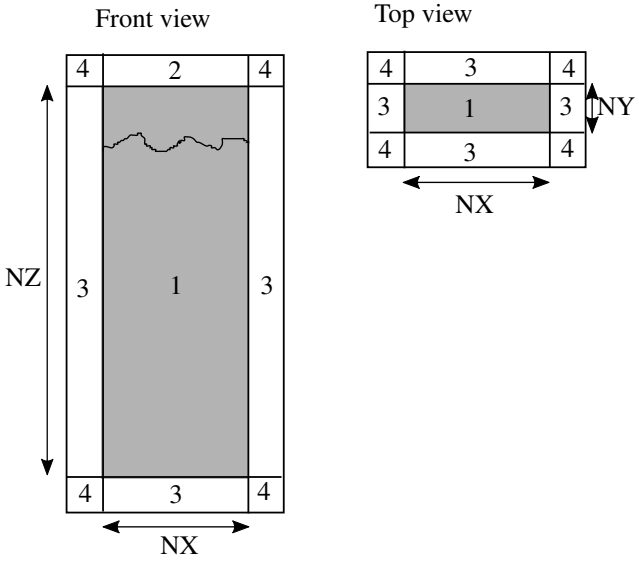

Figure 3: Boundary conditions for the VOF-DBM; Front view at j=NY/2 and top view for cells k=2 to k=NZ-1.

The turbulence in the liquid phase due to bubbly flow is taken into account by using a sub-grid scale model proposed by Vreman (2004) for the eddy viscosity.

Bubble coalescence is accounted for based on the model proposed by Sommerfeld *et al.* (2003). The collision time is determined by the relation reported by Allen and Tildesley (1989). Film drainage time for coalescence to occur is calculated based on the model of Prince and Blanch (1990). When the contact time is less than the film drainage time coalescence does not occur and the bubbles simply bounce. Otherwise, they coalesce. A detailed description of the model can be found in Darmana *et al.* (2005). Bubble

Table 2: Flag meaning for cell boundary conditions

Flag	Boundary conditions
1	Interior cell, none specified
2	Prescribed pressure cell, free slip
3	Impermeable wall, no slip, Neumann for species
4	Corner cell, none specified

breakup occurs if the inertial force exceeds the surface tension forces, the ratio of which can be represented as Weber number. The critical Weber number for breakup to occur is 12 as determined by Jain *et al.* (2014). Based on this, a binary breakup model is considered where after break-up the bigger bubble is placed at the position of the parent bubble and the smaller bubble is placed randomly around the centroid of the bigger bubble.

Wire-mesh and cutting

The wire mesh is present in the middle of the column to cut the bubbles. A simple geometric cutting model proposed by Jain *et al.* (2013) is incorporated to account for cutting the bubbles when they pass the wire mesh. A stochastic factor called cutting efficiency is introduced into the model to characterize the fraction of bubbles that is actually cut by the wire mesh. A cutting efficiency 0 means there is no cutting and a value of 1 means all bubbles are eligible to get cut. The drag that the wire-mesh exerts on the liquid is taken into account in Equation 9 (Jain *et al.*, 2013).

Chemical species equations

The species are accounted for through Y_j which is the mass fraction of species j. Species balances for $N_s - 1$ components are solved simultaneously with appropriate boundary conditions, where N_s is number of components present in the system. The fraction of the last component can be derived from the overall mass balance.

$$\frac{\partial}{\partial t}\left(F\varepsilon_f\rho_f Y_j\right) + \nabla\cdot\left(F\varepsilon_f\left(\rho_l \mathbf{u} Y_j - \Gamma_{j,eff}\nabla Y_j\right)\right) = \left(\dot{M}^j{}_{b\to l} - \dot{M}^j_{l\to b}\right) + F\varepsilon_f S_{R,j} \tag{16}$$

$$\sum_{j=1}^{N_S} Y_j = 1 \tag{17}$$

S_{Rj} is the source term accounting for the production or consumption of species j due to chemical reaction.

The mass transfer is given by:

$$\dot{m}^j_b = Ek^j_l A_b \rho_l (Y^{j*}_l - Y^j_l) \tag{18}$$

Where the mass transfer coefficient k_l is calculated through a Sherwood correlation. Several mass transfer correlations are available in literature for bubbly flows. Brauer (1981) gives a correlation for ellipsoidal bubbles accounting for the shape of the bubble due to the deformations caused by liquid flow around bubbles:

$$Sh = 2 + 0.015 \times Re_B^{0.89} Sc^{0.7} \tag{19}$$

The correlation for the enhancement factor (E) provided by Westerterp *et al.* (1987) is used as proposed by Darmana *et al.* (2005).

RESULTS

Visual observation

Images are obtained using a high-speed camera operated at 50 Hz, for a velocity of 5-30 mm/s for different wire meshes and the Sulzer packing(SMV). Fig. 4 shows the images of bubbly flow in a MSBC for three different configurations, such as no internals, with mesh (3.6 mm mesh opening) and Sulzer packing. The images shown are for the mid section at a superficial gas velocity of 15 mm/s. In Fig. 4b & 4c, there are small bubbles present above and below the mesh/Sulzer packing. The presence of small bubbles also increases with increasing superficial gas velocities as a consequence of bubble break-up. In Fig. 4a, for the case without internals the bubbles are homogeneously distributed in the column with some big bubbles. When comparing the three figures (Fig. 4a, 4b & 4c), it is evident that the bubble cutting occurs in the presence of internals.

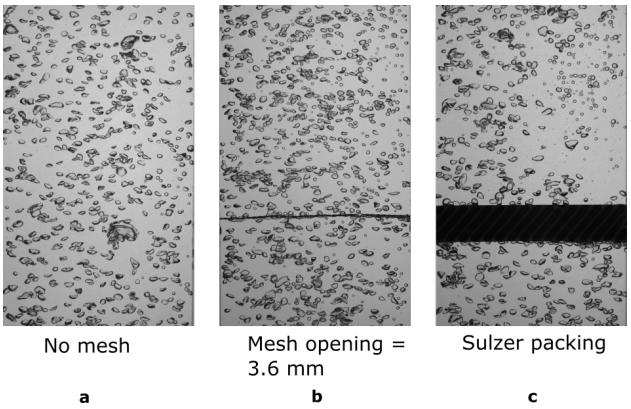

Figure 4: Images of bubbly flow in the MSBC with no mesh, 3.6 mm mesh opening and Sulzer packing at superficial gas velocity 15 mm/s.

Effect of internals

It is important to note that for Fig. 5 and Fig. 6, time-averaging is done for a duration of 4 seconds (i.e. between 10 to 14 seconds after the CO_2 flow starts in the column) for all superficial gas velocities and mesh openings. It is reasonable to assume that the hydrodynamics of the bubbly flow does not change within such a short time span, as there is a very small change in pH. This assumption enables comparison of the cutting behavior of different internals at a particular superficial gas velocity.

The effect of mesh configuration is studied for three different wire mesh openings (i.e. for 2.7 mm, 3.3 mm and 3.6 mm) for comparison with the no mesh case and Sulzer packing. The time-averaged Sauter mean diameter and volumetric probability density function are plotted in Fig. 5 and Fig. 6 respectively. The Sauter mean diameter is ratio of volume to surface area of the detected bubbles from the three different image sections. It is used to evaluate the mass transfer performance of the wire meshes/packing used in the MSBC.

Fig. 5 shows the time averaged Sauter mean diameter plotted vs height of the MSBC, for different configurations of internals. The meshes/packings perform much better than the no mesh case, as there is approximately 1 mm drop in bubble diameter after the location of mesh/packing (i.e. 0.26 m).

The bubble cutting is also evident in Fig. 6, which shows the time-averaged volumetric probability density vs diameter for different column configurations. Sulzer packing performs the best in terms of resizing the bubbles. Amongst the wire meshes the mesh with 3.6 mm opening performs the best.

This can also observed in the plot of pH vs time for different cases as shown in Fig. 7, as the pH curve for the 3.6 mm mesh opening and Sulzer packing drops fast to reach pH 7 in 70 seconds. The MSBC with no mesh configuration takes almost 90 to 100 seconds for reaching pH 7 at same velocity. Hence the pH decay curves show that MSBC with internals perform much better than the configuration with no internals for a reaction limited by gas-liquid mass transfer. It should be observed that although Sulzer packing has better cutting than the 3.6 mm mesh it has a similar performance in terms of mass transfer.

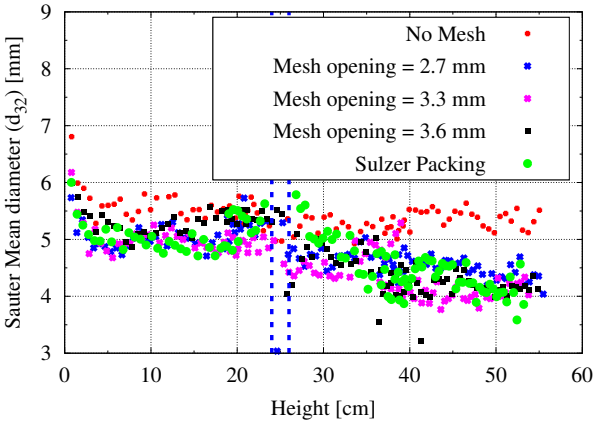

Figure 5: Sauter mean bubble diameter vs height for varying mesh types at superficial gas velocity 25 mm/s. Position of mesh(0.26 m) and packing(0.24 to 0.26 m) is indicated by blue dashed line.

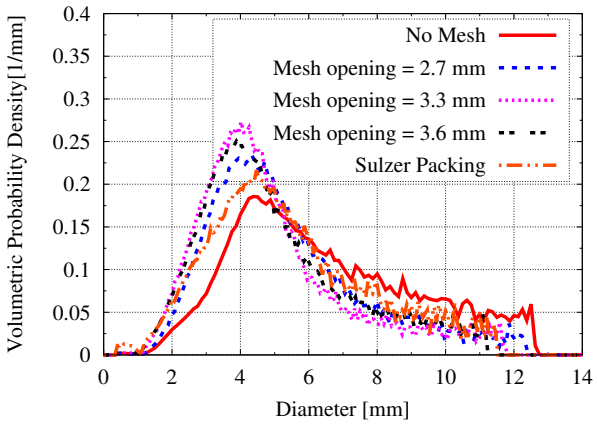

Figure 6: Volumetric probability density function vs diameter in varying mesh types at superficial gas velocity 25 mm/s in the top section (0.42 to 0.60 m).

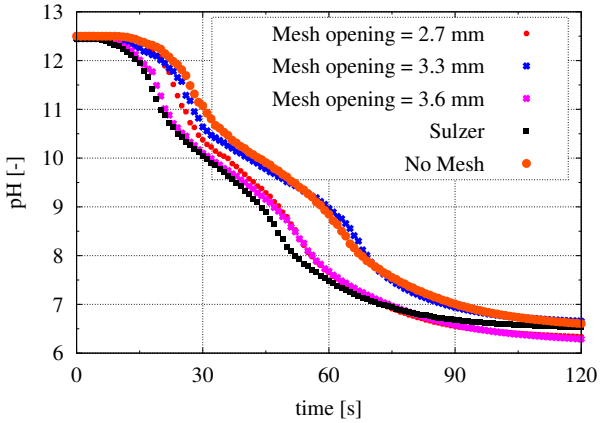

Figure 7: pH vs time curve for different mesh types at superficial gas velocity 20 mm/s.

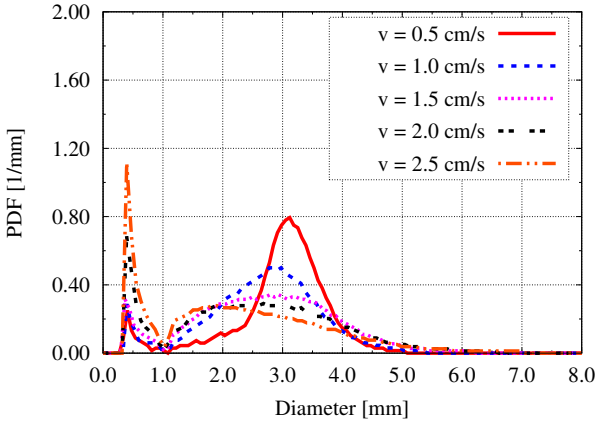

Figure 8: Bubble size distribution with varying superficial gas velocities (5 to 25 mm/s) for mesh opening 3.6 mm in the top section (0.42 to 0.60 m).

Effect of superficial gas velocity

The time averaging of bubble size distributions are done for a duration of 4 seconds (i.e. between 10 to 14 seconds after the CO_2 flow starts in the column) for all superficial gas velocities and mesh openings. It is reasonable to assume that the hydrodynamics of the bubbly flow does not change within such a short time span, as there is a very small change in pH.

The effect of superficial gas velocity on the time-averaged bubble size distribution can be seen in Fig. 8. At 5 mm/s, two peaks can be observed. The left peak corresponds to very small bubbles (less than 1 mm in diameter) and the larger peak corresponds to the average bubble size (3 mm diameter). The bimodal nature of distribution is due to the formation of very small bubbles resulting from breakup at the free surface, which are subsequently dragged down into the column by liquid circulation. It can be seen that as the velocity is increased the distribution becomes flatter due to bubble coalescence and breakup until 15 mm/s. For higher velocities, the distribution of the second peak tends to shift towards smaller bubbles as a result of enhanced bubble cutting and breakup. This trend is general for all cases with and without internals. However with the presence of internals the bubble cutting has an added impact on the bubble size distribution.

Simulation

Simulations were conducted for five superficial gas velocities to compare with experiments carried out with a wire mesh of 3.6 mm opening. The mesh was placed at a height of 0.27 m from the bottom. A cutting efficiency of 0.1 was used for the simulations. The results of Sauter mean diameter, bubble size distribution, pH and gas holdup will now be discussed for a superficial gas velocity of 15 mm/s.

Fig. 9 shows the comparison of the Sauter mean diameter between experiments and simulations. The nature of the cutting in the model of Jain *et al.* (2013) is abrupt and occurs for all cases, whereas in experiments the cutting is gradual. The discrepancy between experiments and simulations is due to the high bubble coalescence rate before the mesh region. It can also be noticed that the initial bubble diameter in the simulations is set to 4 mm and it should be increased.

A comparison of the bubble size distributions is shown in Fig. 10. It can be seen that the first peak of the experiments is not well captured in the simulations, as we do not model the violent breakup at the top interface. Experiments cannot detect bubbles below 0.3 mm whereas the simulation can keep track of these very small bubbles, resulting in a smoother initial curve in the simulations. However, the simulation captures the overall trend of the experiments fairly well.

Fig. 11 shows a comparison of the pH histories obtained experimentally and numerically. It can be seen that the two inflection points are well matched, which indicates that the reaction kinetics are a good description of reality. But the model under-predicts the pH decay rate. This could be due to the presence of large bubbles which in turn lead to lower rate of mass transfer. The time taken for neutralization is well captured by the model for all superficial gas velocities.

The gas holdup values match well between experiments and simulations and the error stays below 10% for all cases, as shown in Fig. 12, except at time t=0. The holdup predicted by simulations is lower than the experimentally determined value at time t=0, as a result of the differences in the startup procedure for chemisorption. In simulations, the hydrodynamics calculations are performed for a N_2 - $NaOH$ system until numerical effects disappear and then the system is switched to chemisorption at time t=0. The gas in reactor is completely switched to CO_2 and it reacts with $NaOH$, leading to disappearance of bubbles throughout the reactor. This causes a decrease in the gas holdup at the onset of chemisorption. However, in the experiments few N_2 bubbles are still present in the bubble column after startup in addition to CO_2 gas. As the N_2 bubbles do not react with $NaOH$, they have an added contribution to the gas holdup until they leave the column. The deviation in gas holdup predicted by simulations and experiments, lowers with time as seen in Fig. 12.

CONCLUSIONS

In this work, a detailed analysis of the micro-structured bubble column (MSBC) has been performed for the case of chemisorption of CO_2 into $NaOH$. Different internals

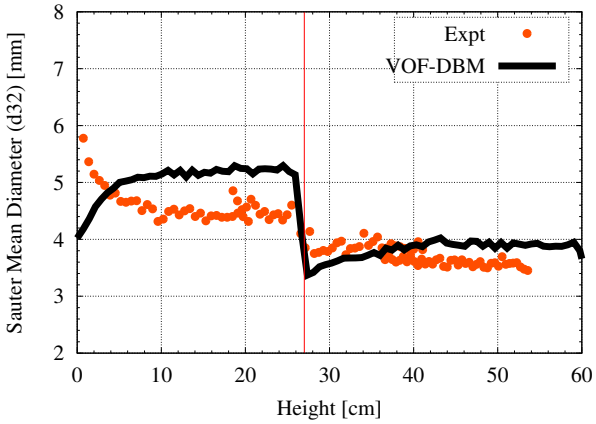

Figure 9: Sauter mean diameter (time averaged) as a function of column height with superficial gas velocity 15 mm/s for mesh opening 3.6 mm.

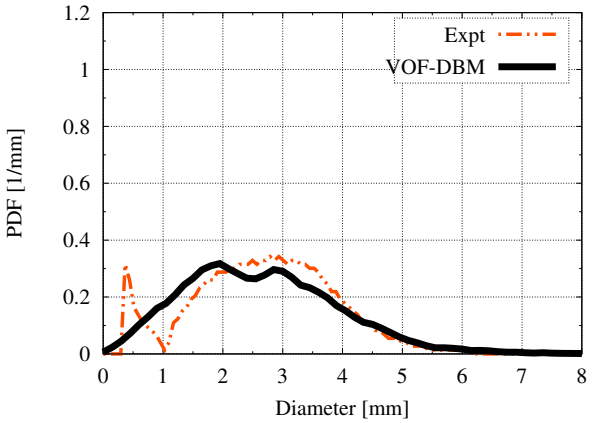

Figure 10: Bubble size distribution with superficial gas velocity 15 mm/s for mesh opening 3.6 mm.

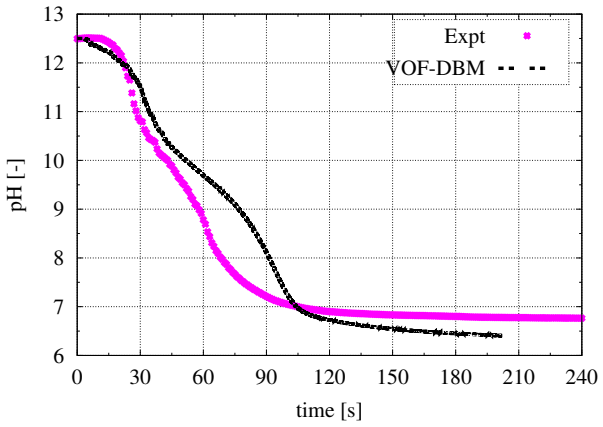

Figure 11: pH vs time with superficial gas velocity 15 mm/s for mesh opening 3.6 mm.

such as a wire mesh and a Sulzer packing (SMV) have been tested in the MSBC experimentally to characterize the bubble cutting and mass transfer performance. The Sulzer packing and the wire mesh with a 3.6 mm opening shows good cutting characteristics as seen in their bubble size distribution. This increases the interfacial area in turn resulting in an increased gas holdup and better mass transfer performance. Since the chemisorption is mass transfer limited the reaction times are found to decrease significantly in presence of the internals.

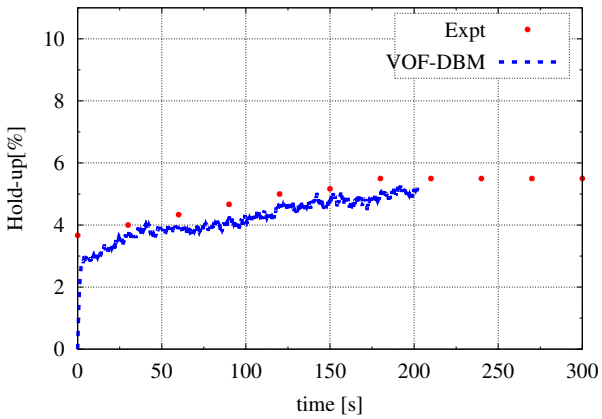

Figure 12: Gas holdup vs time with superficial gas velocity 15 mm/s for mesh opening 3.6 mm.

The VOF-DBM model is integrated with equations for chemisorption and validated with experiments. An optimal value of the cutting efficiency was determined and the results are compared with experiments. The major drawback of the cutting model is that it is independent of the superficial gas velocity. Therefore an effort should be made to improve the cutting model by using closures from direct numerical simulations (DNS).

ACKNOWLEDGEMENTS

The authors would like to thank the European Research Council for its financial support, under its Starting Investigator Grant scheme, contract number 259521 (CuttingBubbles).

REFERENCES

ALLEN, M.P. and TILDESLEY, D.J. (1989). *Computer simulation of liquids*. Oxford university press.

BAIRD, M.H.I. (1992). "Bubble column reactors. By W.-D. Deckwer, Wiley, New York, 1991". *AIChE Journal*, **38(8)**, 1305–1305.

BRAUER, H. (1981). "Particle/fluid transport processes". *Progress in Chemical Engineering*, **19**, 81–111.

DARMANA, D. *et al.* (2005). "Detailed modeling of hydrodynamics, mass transfer and chemical reactions in a bubble column using a discrete bubble model". *Chemical Engineering Science*, **60(12)**, 3383–3404.

DEEN, N.G. *et al.* (2000). "Bubble Columns". *Ullmann's Encyclopedia of Industrial Chemistry*, 34. Wiley-VCH Verlag GmbH & Co.

JAIN, D. *et al.* (2013). "Discrete bubble modeling for a micro-structured bubble column". *Chemical Engineering Science*, **100**, 496–505.

JAIN, D. *et al.* (2014). "Numerical study of coalescence and breakup in a bubble column using a hybrid volume of fluid and discrete bubble model approach". *Chemical Engineering Science*, **119**, 134–146.

LAU, Y.M. *et al.* (2013a). "Development of an image

measurement technique for size distribution in dense bubbly flows". *Chemical Engineering Science*, **94**, 20–29.

LAU, Y.M. *et al.* (2013b). "Experimental study of the bubble size distribution in a pseudo-2D bubble column". *Chemical Engineering Science*, **98**, 203–211.

MEYER, F. (1994). "Topographic distance and watershed lines". *Signal Processing*, **38(1)**, 113–125.

OTSU, N. (1975). "A threshold selection method from gray-level histograms". *Automatica*, **11(285-296)**, 23–27.

PRINCE, M.J. and BLANCH, H.W. (1990). "Bubble coalescence and break-up in air-sparged bubble columns". *AIChE Journal*, **36(10)**, 1485–1499.

SOMMERFELD, M. *et al.* (2003). "Euler/Lagrange calculations of bubbly flows with consideration of bubble coalescence". *Canadian Journal of Chemical Engineering*, vol. 81, 508–518.

SUJATHA, K.T. *et al.* (2015). "Experimental studies of bubbly flow in a pseudo-2d micro-structured bubble column reactor using digital image analysis". *Chemical Engineering Science*, **130(0)**, 18 – 30.

VAN SINT ANNALAND, M. *et al.* (2005). "Numerical simulation of gas bubbles behaviour using a three-dimensional volume of fluid method". *Chemical Engineering Science*, **60(11)**, 2999–3011.

VREMAN, A.W. (2004). "An eddy-viscosity subgrid-scale model for turbulent shear flow: Algebraic theory and applications". *Physics of Fluids*, **16(10)**, 3670.

WESTERTERP, K.R. *et al.* (1987). *Chemical reactor design and operation*, vol. 84. Wiley Chichester.